Effective field theory of interacting π electrons

J. D. Barr* and C. A. Stafford
Department of Physics, University of Arizona, 1118 East Fourth Street, Tucson, Arizona 85721, USA

J. P. Bergfield
Nano-Science Center and Department of Chemistry, University of Copenhagen, Universitetsparken 5, 2100 Copenhagen Ø, Denmark
(Received 10 November 2011; revised manuscript received 1 August 2012; published 4 September 2012)

We develop a π-electron effective field theory (π-EFT) wherein the two-body Hamiltonian for a π-electron system is expressed in terms of three effective parameters: the π-orbital quadrupole moment, the on-site repulsion, and a dielectric constant. As a first application of this π-EFT, we develop a model of screening in molecular junctions based on image multipole moments, and use this to investigate the reduction of the HOMO-LUMO gap of benzene. Beyond this, we also use π-EFT to calculate the differential conductance spectrum of the prototypical benzenedithiol-Au single-molecule junction and the π-electron contribution to the van der Waals interaction between benzene and a metallic electrode.

DOI: 10.1103/PhysRevB.86.115403 PACS number(s): 73.63.Rt, 31.15.bu, 34.35.+a, 85.65.+h

I. INTRODUCTION

Owing to the profound versatility of the carbon-carbon bond, organic molecules form the basis for a myriad of potential nanotechnology applications. Many of these make use of the ability of conjugated organic molecules to conduct electricity, in which case the system of delocalized π electrons plays a role analogous to that of the conduction band in a conventional semiconductor. In such devices, the most important degrees of freedom from a technological perspective are those associated with these current-carrying π electrons.

The main motivation of the present work is to derive a model Hamiltonian for π-electron systems to facilitate the study of many-body effects on transport through molecular heterojunctions. The standard paradigm for molecular junction transport calculations involves local or semilocal approximations to density functional theory (DFT) combined with nonequilibrium Green's functions (NEGF). This DFT-NEGF approach[1] has tremendous advantages in terms of computational efficiency and chemical realism. However, it has notorious difficulties describing the energetics most relevant for electron transport, namely the energy level alignment between molecule and metal electrodes, and the fundamental (or HOMO-LUMO) gap. Some possible underlying reasons for this are (i) the failure to include nonlocal correlations responsible for screening of intramolecular interactions by nearby metal electrodes,[2,3] (ii) self-interaction error,[4–7] and (iii) omission of the derivative discontinuity[8,9] needed to describe the quantization of the molecular charge within the junction.[10] Self-consistent many-body perturbation theory[11] is able to overcome hurdles (i) and (ii), but still leaves (iii) as an open problem.

An alternative approach is to formulate a model including only the degrees of freedom essential to describing the π-electron dynamics, thereby reducing the overhead associated with an exact treatment of interactions within the junction. Electron transport can then be treated using many-body Green's function techniques,[12,13] the master equation approach,[14–18] or quantum impurity solvers.[19] This procedure begins with the observation that processes in systems of π electrons take place at characteristic length, energy, and time scales all ultimately dictated by the strength of the π-electron bond. Intuitively, one expects that only degrees of freedom with scales comparable to these need to be explicitly included. Semiempirical models based on this notion have been in use for over fifty years,[20–23] and work to improve their accuracy is ongoing.[24–26] However, since these are based on *ad hoc* parametrizations[22,24–27] of interparticle Coulomb interactions that do not satisfy Maxwell's equations, it is difficult to extend such techniques to include effects such as the screening of intramolecular interactions by the electrodes in molecular junctions.

In contrast to this, effective field theory (EFT) provides a concise, systematic method of constructing a π-electron Hamiltonian starting from first principles by performing an expansion in a small parameter and then imposing symmetry constraints. The result contains a few physically meaningful parameters, which are then renormalized to include the aggregate effect of the degrees of freedom not explicitly retained. In this article we proceed along these lines, first expanding the full electronic Hamiltonian of a conjugated organic molecule in a basis of atomic orbitals and then dropping terms involving energies far from the π-electron bond energy.

Imposing symmetry constraints and performing an expansion in powers of the interatomic bond length then allows us to construct an effective Hamiltonian for the π electrons in a conjugated organic molecule that accounts for the effects of σ electrons virtually.[28] As an example of this, we consider the particular case of gas-phase benzene, for which we formulate an effective Hamiltonian with only four adjustable parameters: the on-site repulsion U, the nearest-neighbor hopping matrix element t, a dielectric constant ϵ, and the π-electron quadrupole moment Q. In principle, these could then be renormalized *ab initio*, e.g., by using perturbation theory to freeze out degrees of freedom far from the π-electron energy scale; however, since this is tedious and would not enhance the predictive power of our model, we instead fit the parameters directly to experiment.

Next, we show how screening from metallic electrodes can be incorporated into this scheme without introducing additional parameters by considering the multipole moments

of image charge distributions. We then use this method of screening to calculate the screened HOMO-LUMO gap of benzene near a metallic electrode, as well as to formulate a realistic model of a gold-benzenedithiol-gold junction, including effects arising from the presence of the thiol side groups. The differential conductance spectrum of the junction is calculated as a function of the gate and bias voltages in the experimentally relevant regime,[30] exhibiting the characteristic diamond-shaped features[12] indicative of quantized charge on the molecule within the junction. Finally, we also use this π-electron effective field theory (π-EFT) to compute the π-electron contribution to the van der Waals interaction between benzene and a metallic electrode.

II. BARE HAMILTONIAN

Using the Born-Oppenheimer approximation, the one-body term in the electronic Hamiltonian for an isolated molecule can be written as

$$H^{(1)} = \sum_{\sigma} \int d^3x\, \psi^{\dagger}_{\sigma}(\vec{x}) \left(\frac{-\hbar^2}{2m} \nabla^2 + V \right) \psi_{\sigma}(\vec{x}), \tag{1}$$

where V is the interaction between the electrons and the atomic nuclei. The operator that creates an electron with spin σ in the nth element of a basis of atomic orbitals $\{\phi_n\}$ can be expressed as

$$d^{\dagger}_{n\sigma} = \int d^3x\, \phi_n(\vec{x}) \psi^{\dagger}_{\sigma}(\vec{x}).$$

Multiplying this by the inverse of the overlap matrix $S_{nm} = \langle \phi_n | \phi_m \rangle$ and summing over m implies

$$\begin{aligned} \sum_m d^{\dagger}_{n\sigma} S^{-1}_{nm} \phi^*_m(\vec{x}) &= \int d^3x' \sum_m \phi_n(\vec{x}') S^{-1}_{nm} \phi^*_m(\vec{x}) \psi^{\dagger}_{\sigma}(\vec{x}') \\ &= \psi^{\dagger}_{\sigma}(x), \end{aligned} \tag{2}$$

where we have made use of the completeness relation for a nonorthogonal basis:[31]

$$\sum_{nm} \phi_n(\vec{x}') S^{-1}_{nm} \phi^*_m(\vec{x}) = \delta(\vec{x} - \vec{x}').$$

Combining Eqs. (1) and (2) then gives

$$H^{(1)} = \sum_{nm\sigma} \mathcal{H}_{nm} d^{\dagger}_{n\sigma} d_{m\sigma}, \tag{3}$$

where

$$H^{(1)}_{nm} = \int d^3x\, \phi^*_n(\vec{x}) \left(\frac{-\hbar^2}{2m} \nabla^2 + V \right) \phi_m(\vec{x}) \tag{4}$$

and

$$\mathcal{H}_{nm} = \sum_{kl} S^{-1}_{nk} H^{(1)}_{kl} \left(S^{-1}_{ml} \right)^*. \tag{5}$$

If we keep only nearest-neighbor terms this reduces to the Hückel Hamiltonian

$$H^{(1)} = \sum_n \varepsilon_n d^{\dagger}_{n\sigma} d_{n\sigma} - \sum_{\langle n,m \rangle, \sigma} t_{nm} d^{\dagger}_{n\sigma} d_{m\sigma},$$

where $t_{nm} = \mathcal{H}^{(1)}_{nm}$ and $\varepsilon_n = \mathcal{H}^{(1)}_{nn}$.

Similarly, the two-body term in the electronic Hamiltonian can be written as

$$\begin{aligned} H^{(2)} = \frac{1}{2} \sum_{\sigma\sigma'} \int d^3x_1 d^3x_2\, \psi^{\dagger}_{\sigma}(\vec{x}_1) \psi^{\dagger}_{\sigma'}(\vec{x}_2) \\ \times \frac{e^2}{|\vec{x}_1 - \vec{x}_2|} \psi_{\sigma'}(\vec{x}_2) \psi_{\sigma}(\vec{x}_1), \end{aligned}$$

which, in terms of the atomic orbital basis, is equivalent to

$$H^{(2)} = \frac{1}{2} \sum_{nmlk\sigma\sigma'} \mathcal{U}_{nmlk} d^{\dagger}_{n\sigma} d^{\dagger}_{m\sigma'} d_{l\sigma'} d_{k\sigma}, \tag{6}$$

where

$$U_{nmkl} = \int d^3x_1 d^3x_2\, \phi^*_n(\vec{x}_1) \phi^*_m(\vec{x}_2) \frac{e^2}{|\vec{x}_1 - \vec{x}_2|} \phi_k(\vec{x}_2) \phi_l(\vec{x}_1)$$

and

$$\mathcal{U}_{nmkl} = \sum_{opqr} S^{-1}_{no} S^{-1}_{mp} U_{opqr} \left(S^{-1}_{kq} \right)^* \left(S^{-1}_{lr} \right)^*. \tag{7}$$

Together, Eqs. (3)–(5) and (6)–(7) give the full electronic Hamiltonian from first principles,

$$H = H^{(1)} + H^{(2)},$$

but do so in terms of a basis that is impractically large for use within existing many-body techniques. To overcome this difficulty, in the next section we formulate an effective Hamiltonian in a reduced basis, explicitly retaining only the degrees of freedom necessary to describe the π-electron dynamics.

III. EFFECTIVE HAMILTONIAN

The first step in constructing the effective Hamiltonian is culling elements of the basis that lie far from the energy scale of interest. To this end, we first exclude atomic orbitals that do not participate in chemical bonding (those corresponding to core or excited electrons), which, in a π-electron system, leaves an effective s orbital and three effective p orbitals at each atom. The former hybridize with the effective p_x and p_y orbitals giving rise to three sp^2 hybrids that form the σ bonds between the atoms. The remaining effective p_z orbitals, which, for a planar molecule, cannot hybridize with any of the σ electrons without breaking inversion symmetry, are occupied by one electron on each atom and form π bonds with weaker binding energies. Because of this energy difference we also omit the atomic orbitals participating in the σ bonds, though this approximation could be relaxed at the expense of a larger basis.

The effective Hamiltonian for the remaining effective p orbitals can then be determined using Eqs. (3) through (7) if the effective orbitals are known. In principle, these could be calculated directly, e.g., by using perturbation theory to freeze out the degrees of freedom far from the π-electron energy scale; however, as noted previously we find it more practical to parametrize these expressions by imposing symmetry constraints.

To do this, we work initially in the asymptotic limit where the interatomic bond length is large compared to the size of the effective orbitals. This condition implies that matrix elements

U_{nmkl} with $n \neq l$ or $m \neq k$ and overlap integrals S_{nm} with $n \neq m$ are exponentially small, allowing us to reduce the interaction matrix [Eq. (7)] to

$$\mathcal{U}_{nmkl} = U_{nmkl} = \delta_{nl}\delta_{mk} \int d^3x_1 d^3x_2 \, \frac{e^2|\phi_n(\vec{x}_1)|^2|\phi_m(\vec{x}_2)|^2}{|\vec{x}_1 - \vec{x}_2|} \equiv \delta_{nl}\delta_{mk} U_{nm}, \tag{8}$$

where ϕ_n are now effective instead of bare orbitals. Although it is known[22] that the terms neglected are not *a priori* negligible at typical interatomic distances, it has been suggested that this approximation can be justified by the use of orthogonalized orbitals,[32] and it has been explicitly shown[33] that this is an accurate approximation for π-conjugated systems. Here we offer a simpler perspective more consistent with the spirit of EFT, namely that the neglected terms are accounted for virtually when the parameters in the Hamiltonian are renormalized. We also note that Eq. (8) is equivalent to the "neglect of differential overlap approximation" that has already been used extensively elsewhere, but that in the context of EFT it is simply the requirement that the effective Hamiltonian be local. However, we note here that in order to extend the present work to the case where multiple orbitals (e.g., both σ and π) are centered on the same atom, it would be necessary to include the same-site interaction matrix elements as additional parameters.

Expanding Eq. (8) in powers of the interatomic bond length yields a standard electrostatic multipole expansion, and, if we assume the effective p orbitals possess azimuthal and inversion symmetry, U_{nm} can be parametrized up to the quadrupole-quadrupole interaction in terms of the on-site repulsion U_{nn} and the zz component of the quadrupole moment Q_n associated with each orbital, as well as a dielectric constant ϵ included to account for the polarizability of the σ and core electrons.

Explicitly, this gives

$$U_{nm} = U_{nn}\delta_{nm} + (1 - \delta_{nm})\left(U^{MM}_{nm} + U^{QM}_{nm} + U^{QM}_{mn} + U^{QQ}_{nm}\right) + O(r^{-6}), \tag{9}$$

where U^{MM} is the monopole-monopole interaction, U^{QM} is the quadrupole-monopole interaction, and U^{QQ} is the quadrupole-quadrupole interaction. For two orbitals with arbitrary quadrupole moments Q^{ij}_n and Q^{kl}_m separated by a displacement $\vec{r}$, the expressions for these are

$$U^{MM}_{nm} = \frac{e^2}{\epsilon r}, \tag{10}$$

$$U^{QM}_{nm} = \frac{-e}{2\epsilon r^3} \sum_{ij} Q^{ij}_m \hat{r}_i \hat{r}_j, \tag{11}$$

$$U^{QM}_{mn} = \frac{-e}{2\epsilon r^3} \sum_{ij} Q^{ij}_n \hat{r}_i \hat{r}_j, \tag{12}$$

$$U^{QQ}_{nm} = \frac{1}{12\epsilon r^5} \sum_{ijkl} Q^{ij}_n Q^{kl}_m W_{ijkl}, \tag{13}$$

where

$$W_{ijkl} = \delta_{li}\delta_{kj} + \delta_{ki}\delta_{lj} - 5r^{-2}(r_k\delta_{li}r_j + r_k r_i \delta_{lj} + \delta_{ki} r_j r_l + r_i \delta_{kj} r_l + r_k r_l \delta_{ij}) + 35 r^{-4} r_i r_j r_l r_k$$

is a rank-four tensor that characterizes the interaction of two quadrupoles.[34] Altogether, this provides an expression for the interaction energy that is correct up to fifth order in the interatomic distance.

To further reduce the number of free parameters it is convenient to simplify the effective Hamiltonian by requiring it to satisfy particle-hole symmetry. Although this is not strictly necessary within the context of π-EFT, the success of Pariser-Parr-Pople type semiempirical models—which implicitly assume particle-hole symmetry—suggests that it is a good approximation to do so. Taking this to be the case, Eq. (4) then gives for the one-body Hamiltonian

$$H^{(1)}_{nm} = \int d^3x \, \phi^*_n(\vec{x}) \left(\frac{-\hbar^2}{2m}\nabla^2 + \sum_l V_l(\vec{x}) \right) \phi_m(\vec{x}),$$

where $V_l(\vec{x})$ is the effective potential due to the ionic hole at site l:

$$V_l(\vec{x}) = \int d^3x' \, \frac{-e^2|\phi_l(\vec{x}')|^2}{\epsilon|\vec{x} - \vec{x}'|}.$$

Using Eq. (8) then gives

$$H^{(1)}_{nm} = \delta_{nm}\left(\varepsilon^{(at)}_n - \sum_{l \neq n} U_{nl} \right) + (1 - \delta_{nm}) t_{nm},$$

where we have defined the atomic on-site energy as

$$\varepsilon^{(at)}_n = \int d^3x \, \phi^*_n(\vec{x}) \left(\frac{-\hbar^2}{2m}\nabla^2 + V_n(\vec{x}) \right) \phi_n(\vec{x}).$$

Defining $\rho_n = \sum_\sigma d^\dagger_{n\sigma} d_{n\sigma}$ and rearranging the two-body term then yields

$$H^{(1)} + H^{(2)} = \sum_n \varepsilon^{(at)}_n \rho_n - \sum_{\langle n,m\rangle,\sigma} t_{nm} d^\dagger_{n\sigma} d_{m\sigma} + \frac{1}{2}\sum_{nm} U_{nm}(\rho_n - 1)(\rho_m - 1) + \frac{1}{2}\sum_n U_{nn}\rho_n - \frac{1}{2}\sum_{nm} U_{nm}.$$

Finally, adding the mutual repulsion of the ionic cores $\frac{1}{2}\sum_{n\neq m} U_{nm}$ gives the full effective molecular Hamiltonian:

$$H = \sum_n \varepsilon^{(at)}_n \rho_n - \sum_{\langle n,m\rangle,\sigma} t_{nm} d^\dagger_{n\sigma} d_{m\sigma} + \frac{1}{2}\sum_{nm} U_{nm} q_n q_m + \frac{1}{2}\sum_n U_{nn} q_n,$$

where we have introduced the effective charge operator defined by $q_n = \rho_n - 1$. In conjunction with Eq. (9), this expresses the effective Hamiltonian for an arbitrary π-electron system in terms of the tight-binding matrix t_{nm}, the on-site repulsion U_{nn}, a dielectric constant ϵ, and the π-electron quadrupole moment Q_n.

In the remainder of this paper we focus on benzene as a benchmark system, in which case the Hamiltonian reduces to

$$H = \mu \sum_n \rho_n - t \sum_{\langle n,m\rangle,\sigma} d^\dagger_{n\sigma} d_{m\sigma} + \frac{1}{2}\sum_{nm} U_{nm} q_n q_m, \tag{14}$$

where $U_{nn} = U$ and $Q^{zz}_n = -Q^{xx}_n/2 = -Q^{yy}_n/2 \equiv Q$ by symmetry. The molecular chemical potential μ is fixed by the

experimental ionization energy[35–39] and electron affinity,[40]

$$\mu = \frac{IE - EA}{2} = -4.06 \text{ eV},$$

whereas the four other parameters must be renormalized by fitting to experiment, which is the subject of the following section.

IV. RENORMALIZATION: FITTING THE GAS-PHASE SPECTRUM

We have renormalized the parameters in our effective Hamiltonian for gas-phase benzene by fitting to experimental values that should be accurately reproduced within a π-electron-only model. In particular, we have simultaneously optimized the theoretical predictions of (1) the vertical ionization energy, (2) the vertical electron affinity, and (3) the six lowest singlet and triplet excitations of the neutral molecule.

This was done by exactly diagonalizing Eq. (14) with the interatomic bond length[45] fixed at 1.40 Å. In particular, using the OQNLP algorithm[46] for nonlinear global optimization we minimized the rms relative error of our predictions for the quantities in the first column of Table I. The results of this procedure, which converged to the same solution regardless of initial conditions, are summarized in column two of the same table. The optimal parametrization for the π-EFT was found to be $t = 2.70$ eV, $U = 9.69$ eV, $Q = -0.65\ e\text{Å}^2$, and $\epsilon = 1.56$ with a rms relative error of 4.2 percent.

Also appearing in Table I are the predictions of a recent Pariser-Parr-Pople type semiempirical model[26] as well as those of the original Ohno parametrization.[22,27] Compared to the recent PPP model, π-EFT fits the optical spectrum of gas-phase benzene to a similar degree of accuracy and gives better results for the ionization energy and electron affinity. Moreover, the parameters common to both models have comparable values, namely those given above for our model and those of the model of Castleton *et al.*[26] ($t = 2.64$ eV, $U = 8.9$ eV, and $\epsilon = 1.28$). The π-EFT on-site repulsion is also in qualitative agreement with recent RPA-based calculations of the effective Coulomb repulsion in graphene.[47]

Although our effective quadrupole moment has no direct counterpart in phenomenological models, its value can be compared to the bare quadrupole moment of a hydrogenic $2p_z$ orbital, which is given by

$$Q_{zz} = -24e(a_0/Z)^2, \tag{15}$$

where a_0 is the Bohr radius and $+Ze$ is the nuclear charge. Using this, we find that our π-orbital quadrupole moment corresponds to a hydrogenic p orbital bound by an effective charge of $+3.22e$, or, equivalently, with an effective Bohr radius of 0.16 Å. This is consistent with the expectation that the sp^2 orbitals forming the σ bonds provide only weak screening of the atomic core, which has a net charge of $+4$e. For the purpose of visualization, effective hydrogenic orbitals can also be used to render the average π-electron density $\langle\psi^\dagger(\vec{x})\psi(\vec{x})\rangle$, as shown in Fig. 1.

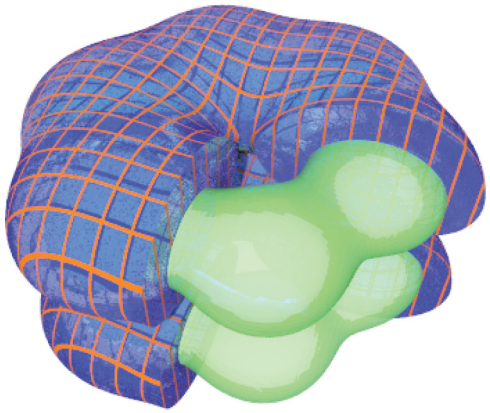

FIG. 1. (Color online) Two isosurfaces of the average π-electron density $\langle\psi^\dagger(\vec{x})\psi(\vec{x})\rangle$ depict the electronic structure of gas-phase benzene within π-EFT.

V. SCREENING BY METALLIC ELECTRODES: THE IMAGE MULTIPOLE METHOD

In this section, we extend the preceding model to include the effect of screening by metallic electrodes, which for simplicity are modeled as planar or spherical conductors. In the regime where the characteristic response time of the electrons in the electrode is much shorter than the timescale of the π-electron dynamics, this can be done using the method

TABLE I. Experimental data for the vertical ionization energy (Refs. 35–39), vertical electron affinity (Ref. 40), and optical spectrum (Refs. 41–44) of gas-phase benzene compared to the predictions of π-EFT, a recent PPP-type model (Ref. 26), and the Ohno parametrization (Refs. 22 and 27). The best-fit parametrization of our π-EFT was determined to be $t = 2.70$ eV, $U = 9.69$ eV, $Q = -0.65\ e\text{Å}^2$, and $\epsilon = 1.56$.

	Exp.[35–44]	π-EFT	PPP (Castleton *et al.*[26])	PPP (Ohno[22,27])
Ionization Energy (eV)	9.23	9.26	9.05	9.78
Electron Affinity (eV)	−1.12	−1.14	−0.93	−1.67
Neutral Spectrum (eV)				
Singlet	4.90	4.87	4.76	4.23
	6.21	6.08	6.30	5.52
	6.93	7.59	6.93	6.81
Triplet	3.93	4.10	3.99	3.52
	4.75	4.92	4.74	4.32
	5.60	6.17	5.84	5.58
rms Relative Error (%)	N/A	4.2	6.0	19.0

of images via a straightforward extension of Eq. (9). This is expected to be the case for conjugated organic molecules in the vicinity of gold electrodes, in which case the metallic plasma frequency[48] $\omega_p \approx 9\ \mathrm{eV}/\hbar$ is large compared to the frequency scale of π excitations $\omega_\pi \approx 2t/\hbar \approx 5\ \mathrm{eV}/\hbar$. The leading order correction to the metallic dielectric function, given by the GW approximation, then goes as $(\omega_\pi/\omega_p)^2 \approx 0.3$. Explicit calculations using the GW approach also suggest that corrections to the image charge method tend to be small for organic molecules adsorbed on a metallic surface.[2]

In the following subsections, the multipole moments of the image charge distribution generated by an orbital near planar and spherical conductors are described. To determine the screened interaction matrix, interactions between these and the orbital multipole moments are included in U_{nm} using Eqs. (10) through (13). Overall, the two-body Hamiltonian should give the energy required to prepare the molecular charge distribution by bringing each of the electrons in from infinity with the electrodes maintained at fixed electrostatic potentials. This can be ensured using a number of different counting schemes, but we take one that ensures a symmetric interaction matrix, namely

$$\tilde{U}_{nm} = U_{nm} + \delta_{nm} U^{(i)}_{nn} + \tfrac{1}{2}(1-\delta_{nm})\left(U^{(i)}_{nm} + U^{(i)}_{mn}\right),$$

where U_{nm} is the unscreened interaction matrix, $U^{(i)}_{nm}$ is the interaction between the nth orbital and the image of the mth orbital, and $\tilde{U}_{nm}$ is the screened interaction matrix. Since the image multipole moments of an orbital change as it is brought in from infinity, one might expect a prefactor of $1/2$ in the second term of the preceding equation; however, this is already present in the Hamiltonian itself.

When multiple electrodes are present, the image of an orbital in one conductor produces images in the other electrodes, resulting in an effect reminiscent of a hall of mirrors. We deal with this by including these "higher order" multipole moments iteratively until the difference between successive approximations of $\tilde{U}_{nm}$ drops below a predetermined threshold. In practice, this procedure converged rapidly.

Within the foregoing scheme, the case where one or more electrodes are maintained at a fixed potential other than zero can be treated straightforwardly by including image charges that contribute to the one-body Hamiltonian rather than to $\tilde{U}_{nm}$. For example, a spherical contact with radius R at potential V can be treated using a hypothetical point charge $q = VR$ at the center of the electrode. This technique is especially useful for transport calculations in the context of molecular junctions, as it provides the full junction Hamiltonian at finite bias, alleviating the need for the phenomenological models of capacitive lead-molecule coupling that have been relied on in the past.[12]

A. Screening by a planar electrode

In classical electrostatics, the image of a charge distribution near a planar conductor is merely the mirror image of the charge distribution itself. Thus an orbital with monopole moment q and quadrupole moment Q^{ij} located a distance r away from a conducting plane produces an image orbital inside the conductor located at depth r with multipole moments $\tilde{q} = -q$ and $\tilde{Q}^{ij} = -\sum_{kl} T_{ik} T_{jl} Q^{kl}$, where T_{ik} is a transformation matrix representing a reflection about a plane parallel to the surface of the conductor, i.e.,

$$T_{ik} = \delta_{ik} - 2\hat{n}_i \hat{n}_k, \tag{16}$$

where $\hat{n}$ is the unit vector normal to the planar surface.

B. Screening by a spherical electrode

An orbital with monopole moment q and quadrupole moment Q^{ij} located a distance r from the center of a spherical electrode with radius R induces an image distribution at $\tilde{r} = R^2/r$ with monopole and quadrupole moments

$$\tilde{q} = -q\frac{R}{r} - \frac{R}{2r^3}\sum_{ij} Q^{ij}\hat{r}_i\hat{r}_j$$

and

$$\tilde{Q}^{ij} = -\left(\frac{R}{r}\right)^5 \sum_{kl} T_{ik} T_{jl} Q^{kl},$$

respectively, where T_{ik} is a transformation matrix representing a reflection about the plane normal to the vector $\hat{r}$, similar to Eq. (16).

Thus the orbital quadrupole moment induces a higher order image monopole moment, as well as an image of itself that is deformed and reflected. An image dipole is also generated, but its interaction with the orbital charge distribution is of order r^{-7} and so we have neglected it here.

VI. SCREENING OF THE HOMO-LUMO GAP

Although π-EFT could be used to study a wide variety of phenomena involving conjugated organic molecules, our primary motivation in formulating it has been to facilitate realistic many-body calculations of transport phenomena in molecular junctions. In particular, while recent semiempirical models[26] reproduce the low-lying excitations of gas-phase benzene, their predictions of quantities relevant to transport, namely the fundamental (or HOMO-LUMO) gap and the optical excitations of the ionized molecule, are less accurate. Moreover, in a molecular junction these quantities are renormalized by screening from metallic electrodes as well as the presence of linker groups not explicitly included in the molecular Hilbert space.

Within π-EFT these effects can be clearly seen: Consider the spectral function of gas-phase benzene, which we evaluate at the many-body level using the nonequilibrium Green's function formalism as described in the Appendix. Figure 2 shows this quantity, along with experimental values for the vertical ionization energy (9.23 eV), vertical electron affinity (-1.12 eV), and the first optical excitation of the cation (3.04 eV). As a guide to the eye, the spectrum has been broadened artificially using a broadening matrix of $\Gamma_{nm} = (0.2\ \mathrm{eV})\delta_{nm}$. As an aside, we note here that the close agreement between the experimental values and the maxima of the spectral function suggests our model is accurate at this energy scale. In particular, the accuracy of the theoretical value for the lowest optical excitation of the cation is noteworthy, as this quantity was not fit during the renormalization procedure but rather represents a prediction of π-EFT.

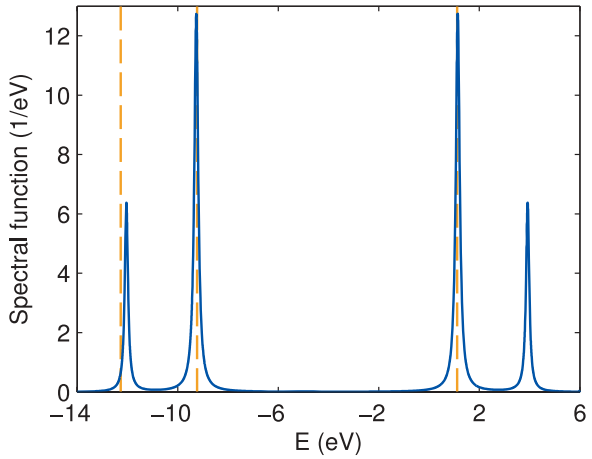

FIG. 2. (Color online) The spectral function of gas-phase benzene broadened artificially as a guide to the eye. The dashed orange lines are fixed by (left to right) the lowest lying optical excitation of the molecular cation (Refs. 36–39, and 49), the vertical ionization energy of the neutral molecule (Refs. 35–39), and the vertical electron affinity of the neutral molecule (Ref. 40).

Screening effects become evident when the molecule is brought into proximity with the surface of a planar electrode. Figure 3 shows the reduction of the ionization energy and electron affinity as a function of electrode-molecule distance in this scenario, and the HOMO-LUMO gap, given by IE − EA, is reduced commensurately. These results, based on the image multipole method, are also consistent with recent GW-based investigations of screening.[2,3]

We also considered the prototypical benzene-gold junction, consisting of benzene linked to two gold electrodes via thiol side groups. Although this junction can occur with a wide variety of different geometries, in this example we have taken the configuration shown in Fig. 4. The electrodes are modeled as metallic spheres with radii of 0.5 nm, and the partially ionic character of the gold-sulfur bond has been accounted for by placing point charges of $-0.67e$ at the locations of the sulfur atoms. The latter value was determined in conjunction with the tunneling-width matrix ($\Gamma_{11} = \Gamma_{44} = 0.44$ eV) via a simultaneous fit of the experimental thermopower[50] and conductance,[51] using the techniques described in the Appendix. The upper panel of Fig. 5 shows the spectral function for this junction in the simple case where the tunneling-width matrix is the same as in Fig. 2, a choice which simplifies comparison of the two cases.

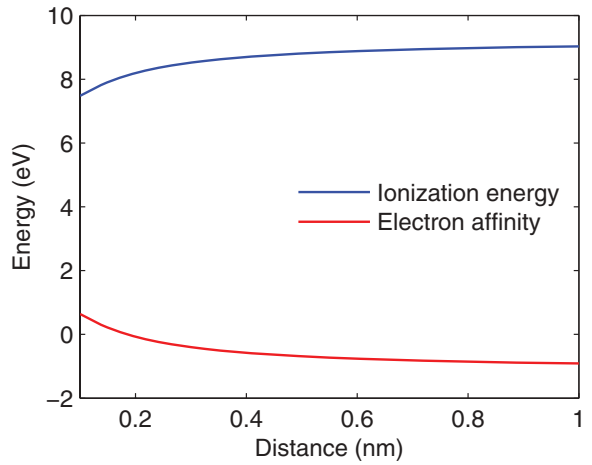

FIG. 3. (Color online) The ionization energy and electron affinity of benzene oriented parallel to the surface of a screening plane, shown as a function of distance.

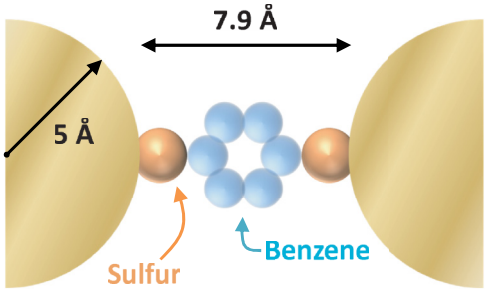

FIG. 4. (Color online) The geometry (Refs. 52 and 53) for the benzenedithiol junction associated with the spectral function shown in Fig. 5. The electrodes have been placed so that the screening surface lies one covalent radius (Ref. 54) beyond the position of the outermost gold nuclei, a convention that has been investigated elsewhere (Ref. 55) in the context of atom-surface van der Waals interactions.

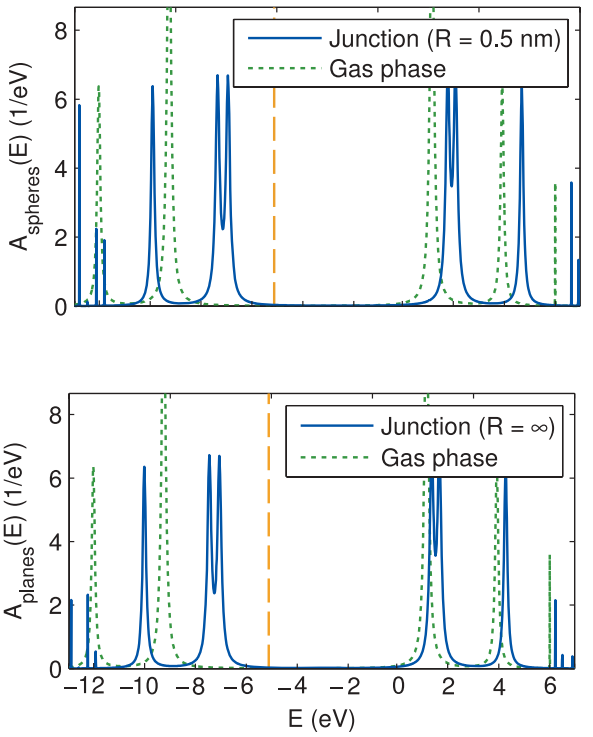

FIG. 5. (Color online) Top: The spectral function of the Au-1,4-benzenedithiol-Au junction depicted in Fig. 4 at room temperature, together with the gas-phase density of states from Fig. 2. To facilitate comparison, the same broadening has been used in both cases. The dashed orange line at −5.1 eV indicates the position of the experimental chemical potential of clean gold (Ref. 56). Bottom: The spectral function of the same junction with planar instead of spherical electrodes.

Screening from the electrodes reduces the HOMO-LUMO gap by 12.5 percent as compared to the gas phase, and the dipole formed by the gold-sulfur bond shifts the chemical potential of the molecule up by 1.4 eV. For comparison, we have also calculated the spectral function of the same junction, but with the electrodes modeled as planes (Fig. 5, bottom), in which case the screening is maximal and the HOMO-LUMO gap is reduced by 19 percent. These results are qualitatively consistent with GW-based investigations of screening effects wherein a molecule is adsorbed on a metallic surface,[2,3] as well as with the recent state-of-the-art GW calculations for benzenedithiol-Au junctions.[11] In comparison to Ref. 11, the HOMO and LUMO resonances in Fig. 5 are both shifted slightly upward in energy, but the gap between them is comparable. It should be pointed out that the upward shifts of HOMO and LUMO in our model are due in part to the dipole moments of the S-Au bonds, which are treated phenomenologically in our model, while the screening of the HOMO-LUMO gap is a fundamental effect described by the image multipole method. As compared to models of screening that treat only the π-orbital monopole moment,[57] the reduction of the HOMO-LUMO gap predicted herein is somewhat smaller, presumably owing to the tendency of the monopole-quadrupole and quadrupole-quadrupole interactions to soften short-range Coulomb interactions. For both of the electrode geometries we considered, a splitting of the twofold-degenerate HOMO and LUMO resonances can also be seen, which arises from the interaction between the π electrons and the dipoles associated with the partly ionic gold-sulfur bonds.

We also note that, as compared to DFT-based treatments of similar junctions,[58] the HOMO-LUMO gap seen in Fig. 5 is dramatically larger, consistent with the observation[59] that correlation effects beyond the scope of local DFT must be included to accurately model transport through this junction.

VII. DIFFERENTIAL CONDUCTANCE SPECTRUM

The advantages of a computational approach such as π-EFT combined with many-body NEGF are perhaps most evident in describing transport through a molecular junction far from equilibrium.[30,60–62] For then, not only must the equilibrium energetics of electron addition and removal be described correctly, but the dependence of both processes on both gate and bias voltages must be correct, a significant challenge for conventional approaches.[10] To illustrate the advantages of π-EFT in this context, we have calculated the differential conductance spectrum of a Au-1,4-benzenedithiol-Au junction. Figure 6 shows the absolute value of the differential conductance on a logarithmic scale, calculated as a function of bias voltage and the electrostatic potential on a spherical gate electrode of radius 3 Å centered 5 Å above the benzene ring. The effective electrostatic lever arm of the gate is 0.21 eV/V. The junction geometry is otherwise identical to that depicted in Fig. 4. In Fig. 6, we have used the physical tunneling-width matrix $\Gamma_{11} = \Gamma_{44} = 0.44$ eV.

Of particular note are the diamond-shaped features in the differential conductance spectrum: The charge on the molecule within the junction is quantized and the differential conductance is suppressed within the diamond-shaped regions centered along the horizontal axis due to the phenomenon of Coulomb blockade.[10,12] This is similar to what has been observed experimentally in junctions based on larger dithiolated molecules,[60–62] in which case the charging energy is significantly smaller. To describe this phenomenon within DFT would require a proper treatment of the derivative discontinuity[8,9] far from equilibrium, for which no theory currently exists. To the best of our knowledge, charge quantization effects like these are beyond the scope even of self-consistent many-body perturbation theory, e.g., as in the case of the state-of-the-art DFT + GW approach.[11]

Resonant tunneling through electronic excited states at large bias and suppression of transport at small bias due to destructive quantum interference (blue fringes) are also clearly visible in Fig. 6. This differential conductance spectrum is similar to that obtained previously[12] using a PPP model of the electronic structure. The main differences are that the sizes of the Coulomb diamonds are reduced due to screening from the metal electrodes, and the particle-hole symmetry of the PPP spectrum is broken by the presence of the S-Au dipoles.

VIII. π-ELECTRON CONTRIBUTION TO THE VAN DER WAALS INTERACTION

As a final application of the image-multipole method, we consider the π-electron contribution to the van der Waals interaction between a molecule and a metallic electrode. Experimentally, such interactions are important when a molecule

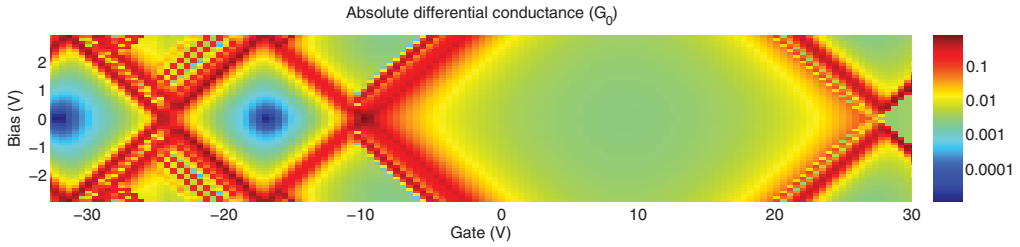

FIG. 6. (Color online) Differential conductance spectrum of a Au-1,4-benzenedithiol-Au junction at room temperature versus gate and bias voltages. The junction geometry, including source and drain electrodes, is depicted in Fig. 4; a spherical gate electrode of radius 3 Å (not shown) is centered 5 Å above the benzene ring. The effective electrostatic lever arm of the gate is 0.21 eV/V. The charge on the molecule within the junction is quantized within the diamond-shaped regions centered on the horizontal axis due to the phenomenon of Coulomb blockade. Resonant tunneling through electronic excited states at large bias and suppression of transport at small bias due to destructive quantum interference (blue fringes) are clearly visible.

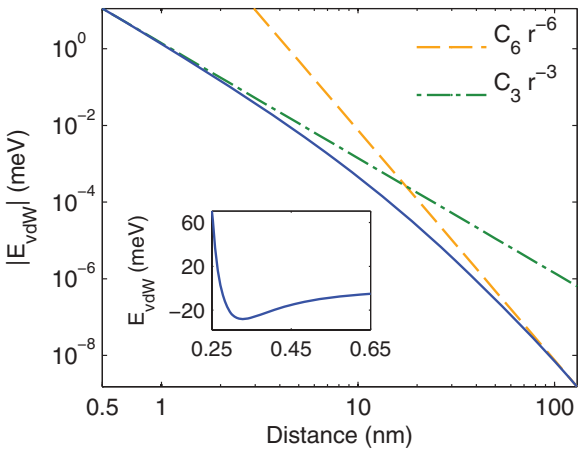

FIG. 7. (Color online) The π-electron contribution to the van der Waals interaction between benzene and a spherical electrode with a radius of 10 nm, plotted as a function of the distance from the conducting surface. At all distances the molecule is oriented parallel to the surface of the electrode. The dashed green and orange lines show the expected asymptotic dependence in the near and far fields, respectively. Inset: The same quantity very near the surface of the electrode, including a phenomenological (Ref. 67) gold-carbon hard-core repulsion.

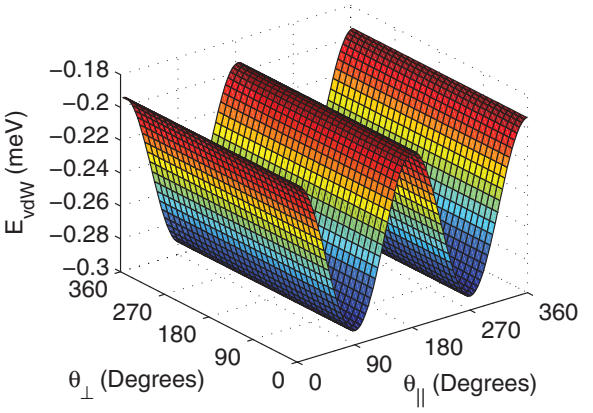

FIG. 8. (Color online) The orientation dependence of the π-electron contribution to van der Waals interaction between a planar electrode and a benzene molecule centered 2 nm from the metal surface. The molecule is initially oriented parallel to the electrode and then rotated by an angle $\theta_\perp$ about the axis perpendicular to the plane of the molecule, followed by a rotation of $\theta_\parallel$ about an axis within the plane of the molecule.

is adsorbed on a metal surface, or in single-molecule junctions in which a molecule bonds directly to metallic electrodes, as in the Pt-benzene-Pt junctions investigated recently by Kiguchi *et al.*[63] Theoretically, the van der Waals interaction also represents a unique challenge in that it is a true many-body phenomenon arising from quantum correlations induced by long-range interactions. As such, it is outside the scope of local approximations to density functional theory, and modeling van der Waals interactions using nonlocal functionals is a topic of ongoing research.[64–66] In contrast to this, the preceding treatment of screening, in conjunction with a full many-body treatment of the π electrons on the molecule, makes it possible to calculate the π-electron contribution to the van der Waals interaction straightforwardly with no extra adjustable parameters.

In particular, by exactly diagonalizing the few-body molecular Hamiltonian with and without the effects of screening included in U_{nm}, it is possible to infer the van der Waals interaction at zero temperature between a molecule and a metallic electrode by comparing the expectation values of the Hamiltonian in these two cases:

$$E_{vdW} = \langle \tilde{H} \rangle - \langle H \rangle.$$

This procedure was carried out at zero temperature for benzene oriented parallel to the surface of a spherical electrode over a large range of electrode-molecule distances, and the results are shown in Fig. 7. When the molecule is near the surface of the electrode $E_{vdW} = -\frac{C_3}{r^3}$, which is the expected asymptotic dependence for the van der Waals interaction between a molecule and a planar conductor. Conversely, when the molecule is far from the electrode $E_{vdW} = -\frac{C_6}{r^6}$, which is the usual asymptotic dependence of the van der Waals interaction as given by the Lennard-Jones potential. A clear transition between the two regimes can be seen around 10 nm, the radius of the electrode. In the near-field region the constant of proportionality predicted by π-EFT is $C_3 \approx 1.56$ eV Å^3. We also investigated the orientation dependence of the van der Waals interaction between a planar electrode and a benzene molecule, as depicted in Fig. 8, which shows a significantly stronger attractive interaction when the plane of the molecule is oriented perpendicular to the surface of the electrode.

The van der Waals coefficient C_3 is fundamentally related to the molecular polarizability tensor α_{ij}. Thus, for an axially symmetric molecule such as benzene, a simplified single-oscillator model can be used to derive semiempirical formulas relating α_{ij} to C_3 with the molecule oriented either parallel or perpendicular to the surface of a planar electrode:[68]

$$C_3^{\parallel} \approx \frac{E_d}{32}(2\alpha_\perp + 2\alpha_\parallel), \tag{17}$$

$$C_3^{\perp} \approx \frac{E_d}{32}(\alpha_\perp + 3\alpha_\parallel). \tag{18}$$

Here E_d is the energy of the principal dipole-allowed optical transition, and $\alpha_\parallel$ and $\alpha_\perp$ are respectively the molecular polarizabilities parallel and perpendicular to its plane of symmetry. As an internal consistency check and to demonstrate that our technique captures the basic physics of the van der Waals interaction, we have calculated these quantities within π-EFT ($E_d = 7.59$ eV, $\alpha_\parallel = 3.24$ Å^3, and $\alpha_\perp = 0.00$ Å^3), and used them to deduce $C_3^{\parallel} \approx 1.54$ eV·Å^3 and $C_3^{\perp}/C_3^{\parallel} = 1.5$, which are in close agreement with the values of C_3 obtained via direct calculation.

Experimentally, $\alpha_\parallel = 12.31$ Å^3, $\alpha_\perp = 6.35$ Å^3, and $E_d = 6.93$ eV for benzene, and in this case Eq. (17) gives $C_3^{\parallel} \approx 8.08$ eV Å^3, which is roughly five times larger than that predicted by π-EFT. This discrepancy can be attributed to the significant contribution of the σ electrons to the molecular polarizability, as evidenced by the large experimental value of $\alpha_\perp$, which arises from σ-π transitions. Consistent with this and the notion that all of the valence electrons contribute more or less equally to the molecular polarizability, the angular average of the π-EFT polarizability, i.e., $\frac{\alpha_\perp + 2\alpha_\parallel}{3}$, is roughly a quarter

of the same quantity calculated using experimental values. This underscores the importance of the σ-electron dynamics in the context of van der Waals interactions, which arise from the long-range spatial correlation of purely virtual processes. In contrast to this, the effect of the σ electrons on real π-π transitions, such as those involved in transport, should be well described by π-EFT. Moreover, as noted previously, the σ-electron dynamics can be explicitly included within effective field theory at the expense of a larger Hilbert space, and we believe that such a $\pi\sigma$-EFT would accurately reproduce the full van der Waals interaction between a conjugated molecule and a metallic electrode.

IX. CONCLUSIONS

We have shown how EFT can be used to provide a concise derivation of an effective Hamiltonian for π-electron systems by performing a multipole expansion, imposing symmetry constraints, and then renormalizing a few adjustable parameters. In particular, we have optimized the parameters appearing in an effective Hamiltonian for gas-phase benzene, Eq. (14), by fitting to experimental data for (1) the vertical ionization energy, (2) the vertical electron affinity, and (3) the six lowest singlet and triplet excitations of the neutral molecule. This procedure yields a fit which is comparable to or better than traditional PPP models[22,26,27] and gives $U = 9.69$ eV for the on-site repulsion, $t = 2.70$ eV for the nearest-neighbor hopping matrix element, $\epsilon = 1.56$ eV for the dielectric constant, and $Q = -0.65\, e\text{Å}^2$ for the π-electron quadrupole moment. These values of U, t, and ϵ are consistent with those used in previous π-electron models,[26,27,47] while Q is a new physical parameter in our approach, which takes the place of the *ad hoc* functional forms assumed in PPP models and governs the corrections to $1/r$ interactions at short distances.

We have also utilized π-EFT to model the screening of intramolecular Coulomb interactions by nearby metallic electrodes. Within our approach, lead-molecule coupling is treated using a two-step process wherein all long-range Coulomb interactions are included nonperturbatively before lead-molecule tunneling is accounted for via Dyson's equation. The ability to include finite bias and screening effects via image multipoles—without additional adjustable parameters—represents a significant advantage of π-EFT over PPP models, which utilize interactions that do not satisfy Maxwell's equations.

In particular, we have shown how π-EFT facilitates a realistic description of the prototypical Au-1,4-benzenedithiol-Au junction, including transport far from equilibrium. The accurate description of ionization potential and electron affinity as poles of the Green's function—and their shifts due to interactions with metal electrodes—sets π-EFT apart from standard DFT-NEGF approaches, and promises to enable accurate transport calculations for junctions involving a variety of conjugated organic molecules. The ability to simultaneously describe Coulomb blockade and coherent quantum transport appears to set our approach apart even from state-of-the-art self-consistent many-body perturbation theory.[11] The main disadvantages of our approach compared to either DFT or DFT + GW are (i) that certain aspects of the junction are described only phenomenologically, such as the linker groups between the molecule and the metal electrodes, and (ii) that a full diagonalization even of the limited Hilbert space of the π electrons scales very poorly. Nonetheless, exact diagonalization of π-EFT should be tractable for conjugated molecules significantly larger than benzene, such as biphenyl or triphenyl, and the use of configuration-interaction techniques such as coupled-cluster singles and doubles should allow its application to still larger molecules. For these systems, π-EFT provides a framework combining an accurate treatment of electron correlation with a higher degree of realism than is present in conventional PPP techniques.

ACKNOWLEDGMENTS

We thank Vincent Lonij for useful discussions. This material is based on work supported by the Department of Energy under Award No. DE-SC0006699.

APPENDIX: MANY-BODY THEORY OF TRANSPORT IN MOLECULAR JUNCTIONS

Within the nonequilibrium Green's function approach to studying transport in molecular junctions, a quantity of central importance is the retarded Green's function G of the molecule coupled to the electrodes. In the energy domain and using matrix notation, this can be expressed via the Dyson equation as

$$G = G_{\text{mol}} + G_{\text{mol}}\Sigma G, \tag{A1}$$

where G_{mol} is the interacting Green's function of the molecule without tunnel coupling to the electrodes, but including long-range Coulomb interactions between the π electrons and their image multipole moments in the leads. The self-energy Σ can be partitioned into the tunneling self-energy Σ_T associated with the lead-molecule bonds, and a correction to the Coulomb self-energy $\Delta\Sigma_C$ arising from lead-molecule coherence:

$$\Sigma = \Sigma_T + \Delta\Sigma_C.$$

Far from resonance and at room temperature $\Delta\Sigma_C \approx 0$, and so in the present context we neglect this correction—an approximation which is justified in detail in Ref. 12. Assuming the leads can be modeled as Fermi liquids with good screening, the electron-electron interactions within them can be neglected and the tunneling self-energy associated with a given electrode can be expressed as[69]

$$\Sigma_T = V g(E) V^\dagger,$$

where $g(E)$ is the retarded Green's function of the lead and V_{nk} are the matrix elements coupling the lead and molecule. In the broadband limit wherein the density of states in the electrodes varies slowly in the vicinity of the metallic Fermi level, the self-energy then reduces to a purely imaginary matrix with no energy dependence:[69]

$$\Sigma_T = -\frac{i}{2}\sum_\alpha \Gamma_\alpha. \tag{A2}$$

Here the tunneling-width matrix Γ_α associated with lead α given is by

$$\Gamma_{n\sigma,m\sigma} = 2\pi\rho(\varepsilon_f) V_n V_m^* \delta_{\sigma\sigma'},$$

where $\rho(\varepsilon_f)$ is the density of states at the metallic Fermi level, and V_n is the matrix element between the nth π orbital in the molecule and the lead states in the vicinity of the Fermi level. The diagonal elements of this equation are equivalent to Fermi's golden rule, with $\mathrm{Tr}\{\Gamma_\alpha/\hbar\}$ giving the rate at which electrons in lead α are being injected into the molecule.

Aside from the self-energy, the other ingredient needed to evaluate Eq. (A1) is the Green's function of the isolated molecule. This is determined exactly by first finding the few-body eigenstates $\{|\nu\rangle\}$ and eigenenergies E_ν of the isolated molecule, and then using these to explicitly evaluate the molecular Green's function:[12,70]

$$G_{\mathrm{mol}} = \sum_{\nu,\nu'} \frac{[P(\nu) + P(\nu')]C(\nu,\nu')}{E - (E_{\nu'} - E_\nu) + i0^+}. \tag{A3}$$

Here $P(\nu)$ is the statistical occupancy of the νth eigenstate, given at equilibrium by the grand canonical ensemble, and

$$C_{n\sigma,m\sigma'}(\nu,\nu') = \langle\nu|d_{n\sigma}|\nu'\rangle\langle\nu'|d^\dagger_{m\sigma'}|\nu\rangle$$

are many-body matrix elements, where, in the present context, $d^\dagger_{m\sigma}$ creates an electron with spin σ in the mth π orbital of the molecule.

Altogether, Eqs. (A1)–(A3) provide a method for obtaining the full interacting Green's function of the molecule coupled to the electrodes, which may then be used to calculate the various physical quantities of interest. For example, the spectral function is given by[69]

$$A(E) = -2\,\mathrm{Im}G,$$

the trace of which is proportional to the effective single-particle density of states:

$$\rho(E) = \frac{1}{2\pi}\mathrm{Tr}\{A\}.$$

Similarly, the elastic transmission function between two electrodes can also be obtained from the full molecular Green's function via the expression

$$T_{\alpha\beta} = \mathrm{Tr}\{\Gamma_\alpha G \Gamma_\beta G^\dagger\},$$

where Γ_α and Γ_β are the tunneling-width matrices associated with leads α and β, respectively. This quantity may then be used to evaluate the various electronic transport quantities of interest,[71] such as the elastic electrical current

$$I^e_\alpha = \frac{-e}{h}\sum_\beta \int dE\; T_{\alpha\beta}(f_\beta - f_\alpha)$$

and elastic thermal current

$$I^Q_\alpha = \frac{1}{h}\sum_\beta \int dE\; (E-\mu_\alpha)T_{\alpha\beta}(f_\beta - f_\alpha)$$

flowing into lead α. Here $f_\alpha(E)$ and μ_α are respectively the Fermi-Dirac distribution and chemical potential associated with lead α.

*barr@physics.arizona.edu

[1] Juan Carlos Cuevas and Elke Scheer, *Molecular Electronics: An Introduction to Theory and Experiment* (World Scientific Publishing Company, Singapore, 2010).

[2] J. B. Neaton, M. S. Hybertsen, and S. G. Louie, Phys. Rev. Lett. **97**, 216405 (2006).

[3] K. S. Thygesen and A. Rubio, Phys. Rev. Lett. **102**, 046802 (2009).

[4] C. Toher, A. Filippetti, S. Sanvito, and Kieron Burke, Phys. Rev. Lett. **95**, 146402 (2005).

[5] San-Huang Ke, H. U. Baranger, and Weitao Yang, J. Chem. Phys. **126**, 201102 (2007).

[6] Aron J. Cohen, Paula Mori-Sánchez, and Weitao Yang, Science **321**, 792 (2008).

[7] C. Toher and S. Sanvito, Phys. Rev. B **77**, 155402 (2008).

[8] J. P. Perdew, R. G. Parr, M. Levy, and J. L. Balduz, Phys. Rev. Lett. **49**, 1691 (1982).

[9] J. P. Bergfield, Z. F. Liu, K. Burke, and C. A. Stafford, Phys. Rev. Lett. **108**, 066801 (2012).

[10] B. Muralidharan, A. W. Ghosh, and S. Datta, Mol. Simul. **32**, 751 (2006).

[11] M. Strange, C. Rostgaard, H. Hakkinen, and K. S. Thygesen, Phys. Rev. B **83**, 115108 (2011).

[12] J. P. Bergfield and C. A. Stafford, Phys. Rev. B **79**, 245125 (2009).

[13] J. Rincón, K. Hallberg, and A. A. Aligia, Phys. Rev. Lett. **103**, 266807 (2009).

[14] J. König, H. Schöeller, and G. Schon, Phys. Rev. Lett. **78**, 4482 (1997).

[15] Herbert Schoeller and Jürgen König, Phys. Rev. Lett. **84**, 3686 (2000).

[16] J. N. Pedersen and A. Wacker, Phys. Rev. B **72**, 195330 (2005).

[17] U. Harbola and S. Mukamel, Phys. Rep. **465**, 191 (2008).

[18] M. Galperin, A. Nitzan, and M. A. Ratner, Phys. Rev. B **78**, 125320 (2008).

[19] D. Bohr, P. Schmitteckert, and P. Wölfle, Europhys. Lett. **73**, 246 (2006).

[20] Rudolph Pariser and Robert G. Parr, J. Chem. Phys. **21**, 767 (1953).

[21] Robert G. Parr, J. Chem. Phys. **33**, 1184 (1960).

[22] Kimio Ohno, Theor. Chim. Acta **2**, 219 (1964).

[23] J. A. Pople, Trans. Faraday Soc. **49**, 1375 (1953).

[24] M. Chandross, S. Mazumdar, M. Liess, P. A. Lane, Z. V. Vardeny, M. Hamaguchi, and K. Yoshino, Phys. Rev. B **55**, 1486 (1997).

[25] Robert J. Bursill, Christopher Castleton, and William Barford, Chem. Phys. Lett. **294**, 305 (1998).

[26] C. W. M. Castleton and W. Barford, J. Chem. Phys. **117**, 3570 (2002).

[27] S. Ramasesha, I. D. L. Albert, and B. Sinha, Mol. Phys. **72**, 537 (1991).

[28] Within EFT, the σ electrons can be included explicitly at the expense of a larger basis, and this may be necessary in order to explain transport in some experiments (Ref. 29).

[29] Latha Venkataraman, Jennifer E. Klare, Iris W. Tam, Colin Nuckolls, Mark S. Hybertsen, and Michael L. Steigerwald, Nano Lett. **6**, 458 (2006).

[30]Hyunwook Song, Youngsang Kim, Yun Hee Jang, Heejun Jeong, Mark A. Reed, and Takhee Lee, Nature (London) **462**, 1039 (2009).
[31]Kristian S. Thygesen, Phys. Rev. B **73**, 035309 (2006).
[32]K. R. Roby, Chem. Phys. Lett. **11**, 6 (1971).
[33]D. Baeriswyl, D. K. Campbell, and S. Mazumdar, in *Conjugated Conducting Polymers*, edited by H. Kiess (Springer-Verlag, Berlin, 1992).
[34]Jesus Hernandez-Trujillo, Miguel Costas, and Alberto Vela, J. Chem. Soc., Faraday Trans. **89**, 2441 (1993).
[35]J. O. Howell, J. M. Goncalves, C. Amatore, L. Klasinc, R. M. Wightman, and J. K. Kochi, J. Am. Chem. Soc. **106**, 3968 (1984).
[36]Branka Kovac, Manijeh Mohraz, Edgar Heilbronner, Virgil Boekelheide, and Henning Hopf, J. Am. Chem. Soc. **102**, 4314 (1980).
[37]Jeffrey A. Sell and Aron Kuppermann, Chem. Phys. **33**, 367 (1978).
[38]Tsunetoshi Kobayoshi, Phys. Lett. A **69**, 105 (1978).
[39]W. Schmidt, J. Chem. Phys. **66**, 828 (1977).
[40]P. D. Burrow, J. A. Michejda, and K. D. Jordan, J. Chem. Phys. **86**, 9 (1987).
[41]Atsunari Hiraya and Kosuke Shobatake, J. Chem. Phys. **94**, 7700 (1991).
[42]John P. Doering, J. Chem. Phys. **51**, 2866 (1969).
[43]Robert P. Frueholz, Wayne M. Flicker, Oren A. Mosher, and Aron Kuppermann, J. Chem. Phys. **70**, 3057 (1979).
[44]E. E. Koch and A. Otto, Chem. Phys. Lett. **12**, 476 (1972).
[45]Koichi Tamagawa, Takao Iijima, and Masao Kimura, J. Mol. Struct. **30**, 243 (1976).
[46]Zsolt Ugray, Leon Lasdon, John Plummer, Fred Glover, James Kelly, and Rafael Marti, INFORMS Journal on Computing **19**, 328 (2007).
[47]T. O. Wehling, E. Şaşıoğlu, C. Friedrich, A. I. Lichtenstein, M. I. Katsnelson, and S. Blügel, Phys. Rev. Lett. **106**, 236805 (2011).
[48]Stefan Linden, Christian Enkrich, Martin Wegener, Jiangfeng Zhou, Thomas Koschny, and Costas M. Soukoulis, Science **306**, 1351 (2004).
[49]P. Baltzer, L. Karlsson, B. Wannberg, G. Ohrwall, D. M. P. Holland, M. A. MacDonald, M. A. Hayes, and W. von Niessen, Chem. Phys. **224**, 95 (1997).
[50]Kanhayalal Baheti, Jonathan A. Malen, Peter Doak, Pramod Reddy, Sung-Yeon Jang, T. Don Tilley, Arun Majumdar, and Rachel A. Segalman, Nano Lett. **8**, 715 (2008).
[51]Xiaoyin Xiao, Bingqian Xu, and Nongjian J. Tao, Nano Lett. **4**, 267 (2004).
[52]Renato B. Pontes, Frederico D. Novaes, Adalberto Fazzio, and Antônio J. R. da Silva, J. Am. Chem. Soc. **128**, 8996 (2006).
[53]Sara Letardi and Fabrizio Cleri, J. Chem. Phys. **120**, 10062 (2004).
[54]Beatriz Cordero, Veronica Gomez, Ana E. Platero-Prats, Marc Reves, Jorge Echeverria, Eduard Cremades, Flavia Barragan, and Santiago Alvarez, Dalton Trans. **2008**, 2832 (2008).
[55]B. N. J. Persson and E. Zaremba, Phys. Rev. B **30**, 5669 (1984).
[56]D. E. Eastman, Phys. Rev. B **2**, 1 (1970).
[57]K. Kaasbjerg and K. Flensberg, Phys. Rev. B **84**, 115457 (2011).
[58]Su Ying Quek, Latha Venkataraman, Hyoung Joon Choi, Steven G. Louie, Mark S. Hybertsen, and J. B. Neaton, Nano Lett. **7**, 3477 (2007).
[59]Su Ying Quek, Hyoung Joon Choi, Steven G. Louie, and J. B. Neaton, Nano Lett. **9**, 3949 (2009).
[60]Sergey Kubatkin, Andrey Danilov, Mattias Hjort, Jerome Cornil, Jean-Luc Bredas, Nicolai Stuhr-Hansen, Per Hedegard, and Thomas Bjornholm, Nature (London) **425**, 698 (2003).
[61]M. Poot, E. Osorio, K. O'Neill, J. M. Thijssen, D. Vanmaekelbergh, C. A. van Walree, L. W. Jenneskens, and S. J. van der Zant, Nano Lett. **6**, 1031 (2006).
[62]A. Danilov, S. Kubatkin, S. Kafanov, P. Hedegard, N. Stuhr-Hansen, K. Moth-Poulsen, and T. Bjornholm, Nano Lett. **8**, 1 (2008).
[63]M. Kiguchi, O. Tal, S. Wohlthat, F. Pauly, M. Krieger, D. Djukic, J. C. Cuevas, and J. M. van Ruitenbeek, Phys. Rev. Lett. **101**, 046801 (2008).
[64]S. D. Chakarova-Käck, E. Schröder, B. I. Lundqvist, and D. C. Langreth, Phys. Rev. Lett. **96**, 146107 (2006).
[65]Jess Wellendorff, Andre Kelkkanen, Jens Jorgen Mortensen, Bengt I. Lundqvist, and Thomas Bligaard, Top. Catal. **53**, 378 (2010).
[66]Biswajit Santra, Angelos Michaelides, Martin Fuchs, Alexandre Tkatchenko, Claudia Filippi, and Matthias Scheffler, J. Chem. Phys. **129**, 194111 (2008).
[67]S. Arcidiacono, J. H. Walther, D. Poulikakos, D. Passerone, and P. Koumoutsakos, Phys. Rev. Lett. **94**, 105502 (2005).
[68]Vincent P. A. Lonij, Catherine E. Klauss, William F. Holmgren, and Alexander D. Cronin, J. Phys. Chem. A **115**, 7134 (2011).
[69]Supriyo Datta, *Electronic Transport in Mesoscopic Systems* (Cambridge University Press, New York, 1997).
[70]Justin P. Bergfield, Joshua D. Barr, and Charles A. Stafford, ACS Nano **5**, 2707 (2011).
[71]Justin P. Bergfield, Michelle A. Solis, and Charles A. Stafford, ACS Nano **4**, 5314 (2010).